

Soft Matter

Accepted Manuscript



This is an *Accepted Manuscript*, which has been through the Royal Society of Chemistry peer review process and has been accepted for publication.

Accepted Manuscripts are published online shortly after acceptance, before technical editing, formatting and proof reading. Using this free service, authors can make their results available to the community, in citable form, before we publish the edited article. We will replace this *Accepted Manuscript* with the edited and formatted *Advance Article* as soon as it is available.

You can find more information about *Accepted Manuscripts* in the [Information for Authors](#).

Please note that technical editing may introduce minor changes to the text and/or graphics, which may alter content. The journal's standard [Terms & Conditions](#) and the [Ethical guidelines](#) still apply. In no event shall the Royal Society of Chemistry be held responsible for any errors or omissions in this *Accepted Manuscript* or any consequences arising from the use of any information it contains.

Cite this: DOI: 10.1039/xxxxxxxxxx

Heterogeneous Vesicles: An Analytical Approach to Equilibrium Shapes

Sangwoo Kim^a and Sascha Hilgenfeldt^aReceived Date
Accepted Date

DOI: 10.1039/xxxxxxxxxx

www.rsc.org/journalname

We develop an analytical model to predict equilibrium shapes of two-component heterogeneous vesicles or capsules. Using a free energy functional including the bending energies of the two components and line tension contributions, the model describes shape transitions between spherical and polyhedral (faceted) states, complementing and extending results of previous numerical simulations. In the parameter space of relative area fraction, bending modulus ratio, and line tension, a region of polyhedral shapes occurs for weak line tension and large bending modulus ratio and is very robust towards changes in the modeling assumptions. At large enough line tension, the spherical shape fragments into two components. Within the polyhedral region, we compare the energies of all regular and semiregular polyhedra, as well as those of arbitrary prismatic shapes. We find that the largest bending modulus ratios together with larger line tension favor polyhedra with small face number as optimal shapes. In this region, we also demonstrate the counter-intuitive result that the most symmetric polyhedra are not energetically optimal, with specific Archimedean solids and specific prismatic shapes beating more isotropic (e.g. Platonic) polyhedra. Furthermore, all polyhedra of lowest energy are found to be three-fold coordinated. The shape transition boundary for polyhedra can be computed analytically. The model can be utilized to predict heterogeneous vesicle shapes and to estimate physical properties of the components constituting observed vesicles.

1 Introduction

The formation of interfaces to divide otherwise homogeneous media into compartments is one of the most fundamental building principles at the root of complex structures in nature and technology. Layered or fiber composites, foams, superlattice structures, confluent biological tissues, individual cells, or cell organelles are only a few examples of materials characterized by the presence of domains and boundaries between these domains. In many of these examples, the domain size is on the micro- or nano-scale, ensuring that interfacial effects are strong or dominant owing to the superior scaling of surface forces over body forces on the small scale. Therefore, we generally see greater uniformity of domain organization and domain shapes on the very small scale, which has enabled researchers to develop elegant descriptions of the shapes and dynamics of objects like vesicles and capsules, formulated largely or entirely in terms of interfacial properties.

Such structures (which we will henceforth refer to as "vesicles", with the understanding that they include other material classes like capsids) are widely employed in nature to accomplish various functions as containers for material transport, as agents of cell

metabolism, or as material compartments. Reflecting this multiple functionality, a rich morphology is reported in previous studies. Despite this complexity, the quantitative theories alluded to above can explain a multitude of equilibrium shapes modeling a vesicle as an elastic thin shell. Recognizing that bending is a dominant deformation mode for a thin shell, Helfrich proposed a free energy functional as the sum of the integral of square mean curvature and Gaussian curvature.¹ According to the Helfrich energy functional, a smooth vesicle shape is favored, avoiding localized curvature, which is energetically costly. However, a number of virus capsids², polymersomes³ and some cationic vesicles⁴ show distinctly polyhedral shapes, often of icosahedral symmetry.

The existence of polyhedral structures can be partly understood through geometric frustration of a curved surface, which can lead to a vesicle of icosahedral symmetry as the energetically most favorable outcome⁵. As shells are made from individual (and often identical) units of very small size, they form a lattice covering the surface. For a planar sheet, a regular triangular lattice (of hexagonal coordination) is the energetic ground state for many simple interactions between the lattice units⁶⁻⁹). However, constructing a regular lattice on a curved surface (to make a closed vesicular structure) necessitates defects by Euler's theorem¹⁰. In particular, the total number of lattice neighbors has to be reduced by twelve

^a Mechanical Science and Engineering, University of Illinois, Urbana-Champaign; E-mail: sascha@illinois.edu

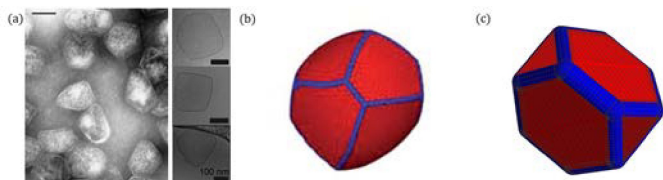


Fig. 1 (a) Experimentally observed polyhedral carboxysomes (left) and assemblies of oppositely charged amphiphiles (right), representing naturally occurring vesicles of heterogeneous composition with non-icosahedral equilibrium shapes; reproduced with permission from^{13,15}. (b) Representative result of the numerical simulations of SVO, demonstrating that such shapes can be obtained from minimization of an energy functional with two shell components. Reproduced with kind permission from the authors²¹. (c) Example of a semi-regular polyhedral shape (a truncated tetrahedron) for which the present work evaluates the energy functional values analytically. In both (b) and (c), the hard material (of higher bending modulus) is colored red and the soft material is blue.

for any regular lattice on a shell of the topology of a sphere. Under generic assumptions about defect core energy, this is realized with least energy expenditure through twelve five-fold defects. While these defects cause stretch energy contributions proportional to R^2 , where R is the vesicle radius, this stretch energy can be released by buckling of the surface, which costs bending energy scaling as $\log(R)$. Hence, the shape transition of the equilibrium state from a sphere to an icosahedron occurs above a critical vesicle size⁵ or, equivalently, a critical Föppl-von-Kármán (FvK) number, $\frac{Y_A R^2}{\kappa}$, where Y_A is the two dimensional Young's modulus of the shell and κ is the bending modulus.

However, the variety of shapes encountered in nature is far greater than just spheres and icosahedra: it has long been known that smooth equilibrium vesicle shapes can have a range of morphologies¹¹, but more recently it has become clear that there is a range of non-icosahedral polyhedra as well, e.g. in an assemblies of oppositely charged amphiphiles^{12,13} and in carboxysomes^{14,15}, see Fig. 1a. The key to understanding this latter diversity of shapes is heterogeneity of the vesicle shell components. Typically, the (at least) two constituents of the shell will separate into domains, and a line tension energy arises at the boundary. The line tension between different materials can induce budding in smooth vesicles^{16–18}. More recent simulation work on polyhedral vesicle shapes has confirmed that polyhedral, distinctly non-icosahedral shapes are energetically favorable for certain ranges of material properties^{19–21}, cf. Fig. 1b. These simulations confirm that in such parameter regimes, the buckling mechanism around twelve defects is unimportant and the relative material properties of the two components become decisive.

While the numerical simulation sheds light on the relation between the vesicle morphology and physical properties, it is desirable to attempt an analytical approach to discuss the overall properties of the material parameter space. This is helpful not only for the understanding of naturally occurring shapes, but for the potential manufacture of capsules of pre-designed shape, as a desired shape can only be realized with materials of certain selected properties. Such an analysis is also capable of quickly and generally comparing the outcomes of different types of models (dif-

ferent energy functionals) to determine whether other physical effects will become important. In this article, we develop such an analysis of heterogeneous (two-component) vesicles using a variety of shape families to find the parameter ranges over which each shape is the energetically most favorable. This approach includes non-icosahedral polyhedral shapes (Fig. 1c) and draws general conclusions on when they are expected to occur over icosahedral (or other regular) polyhedra, or spherical shapes. We will explicitly compare the analytical results with the simulations of Sknepnek, Vernizzi, and Olvera de la Cruz⁽²¹⁾, referred to as SVO in the following). In section 2, the energy functionals and shape approximations used by the model are explained, with general results on the phase diagrams of equilibrium shapes. A comparative discussion on breaking the symmetry of polyhedra is presented in section 3, while an analytical description of the boundaries in parameter space is developed in section 4. Conclusions are presented in section 5.

2 Spherical, Fragmented, and Polyhedral vesicles

In general, the contributions to the total energy of the vesicle can be decomposed as $U_{tot} = U_{bend} + U_{stretch} + U_{vol} + U_{line}$, with separate bending, area stretch, volume elasticity, and line tension contributions (the latter is present because of the heterogeneous composition of the shell and the existence of domain boundaries), see the discussion in SVO. Such a functional can contain a large number of variable parameters, but in the simulations of SVO the area stretch and volume elasticity moduli were chosen large enough so that deviations from the area and volume of a spherical shell were small. This reduced the problem to the desired class of compact, near-isotropic vesicle shapes as opposed to strongly non-compact shapes (e.g. discoid or dog-bone shapes²²). We shall simplify this approach for our analytical purposes by either fixing the overall area of the vesicle shell or the overall volume, representing the respective limit of infinite moduli for these two contributions. We will show that the results are not only very similar to the large-modulus simulations, but that they are quite insensitive to whether area or volume is fixed.

We are primarily interested in the distinction between qualitative classes of shape: not only will we probe the parametric boundaries between spherical vesicles and polyhedra, but we will also allow for the fragmentation of the two-component sphere into two separate objects. Figure 2 shows prototypical representations of the spherical, fragmentation, and polyhedral shape families, with the two materials indicated in red ("hard", higher bending modulus) and blue ("soft", lower bending modulus).

2.1 Energy functional

As in previous numerical studies, the main focus in explaining the phase diagram of shapes is on the competition between a Helfrich bending energy and line tension energy, i.e.,

$$U_{tot} = \frac{1}{2} \kappa_b \iint_A (2H)^2 dA + \kappa_g \iint_A K_g dA + \int_{\partial A} \Gamma dl, \quad (1)$$

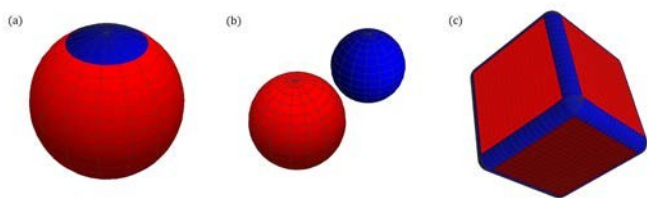


Fig. 2 Representative examples of two-component vesicle shapes. (a) Spherical, (b) Fragmented, (c) Polyhedral (here, a cubic $n=6$ shape). The hard material is colored red and the soft material is blue.

describing the vesicle shape in terms of mean curvature H and Gaussian curvature K_g . The following assumptions and simplifications are employed: (i) The surface area of the vesicle is fixed as that of a sphere of radius R , $A_0 = 4\pi R^2$. It is widely accepted that significant stretching of thin membranes is not likely to happen because it costs far more energy compare to the bending deformation¹. Below, we will also discuss the alternative assumption of constant volume. (ii) The area fraction of soft material is defined as f , where $f = \frac{A_s}{A_0}$. (iii) We follow the common assumption that the bending modulus and the Gaussian bending modulus have the same magnitude but opposite sign for the homogeneous material, $\kappa_b = -\kappa_g = \kappa$. The bending moduli of the soft and hard material are denoted as κ_s and κ_h , respectively. (iv) The line energy at the boundary between soft and hard domains is a constant energy per length Γ . (v) The surface of a vesicle is smooth, i.e., the principal radii of curvature are non-zero everywhere. (vi) the FvK number is small, so that the generation of elementary defects (not present in our continuum model) is an energetically negligible contribution.

We shall report energies below in the non-dimensionalized form $u = U/\kappa_h$; the number of mechanical parameters reduces to two with these assumptions: the bending modulus ratio $\bar{\kappa} = \frac{\kappa_s}{\kappa_h} \leq 1$ and a non-dimensional line tension $\bar{\Gamma} = \frac{\Gamma\sqrt{A_0}}{\kappa_h}$, in analogy with SVO. In the spirit of analyzing representative analytical approximations to the different modes of shape deformation²³, we now compute the energies for the shape families indicated in Fig. 2.

2.2 Spheres

One of the most common vesicle shapes is the sphere because it minimizes bending energy for a given surface area. If the spherical vesicle is composed of two different materials, it will further minimize the total length of the boundary between two materials due to the energy penalty from $\bar{\Gamma}$. This leads to a full segregation of the two materials into a soft and a hard domain (Fig. 2a). The mean curvature and Gaussian curvature are constant everywhere on the sphere, $H = \frac{1}{R}$, $K_g = \frac{1}{R^2}$. Denoting the dimensional length of the boundary as l_{sph} and its dimensionless version as $\bar{l}_{sph} = l_{sph}/\sqrt{A_0}$, the total energy is

$$u_{sph} = \frac{4\pi\bar{\kappa}A_s}{A_0} + \frac{4\pi A_h}{A_0} + \bar{\Gamma}\bar{l}_{sph}, \quad (2)$$

where \bar{l}_{sph} depends on the area fraction f as

$$\bar{l}_{sph} = \sqrt{4\pi f(1-f)}. \quad (3)$$

This results in an explicit expression of u_{sph} as a function of $\bar{\kappa}$, $\bar{\Gamma}$, and f ,

$$u_{sph} = 4\pi[\bar{\kappa}f + (1-f)] + \bar{\Gamma}\sqrt{4\pi f(1-f)}. \quad (4)$$

2.3 Fragmentation

As the line tension $\bar{\Gamma}$ becomes larger and larger, it is eventually energetically favorable to eliminate the boundary between different materials although this fragmentation generates two separate spheres (one of soft and one of hard material), resulting in a higher bending energy. The total energy is then

$$u_{frag} = 4\pi(\bar{\kappa} + 1). \quad (5)$$

2.4 Polyhedral Shapes: Regular Polyhedra

Qualitatively, polyhedral equilibrium states in two-component vesicles are possible because the hard-phase material can relax most of its (higher) bending energy contribution by forming flat facets divided from each other by soft-material regions that form a continuous phase connected along the edges of the polyhedron. It is natural to assume that, in cases where the faceting into polyhedral shapes is energetically favorable, the resulting polyhedra will display high symmetry (e.g. that of Platonic solids). However, the experimental and simulational results do not always bear out that assumption (cf. Fig. 1a,b). In heterogeneous systems, the regularity of the shape will also depend on the area fraction f , and on the fact that a "polyhedron" in this system cannot have idealized one-dimensional edges (whose bending energy would diverge) – the soft-material regions have finite extent and thus vertex and edge relationships are not always unambiguous. We will probe the effect of relaxing symmetries in a later section, but first treat the most regular and symmetric polyhedra.

In polyhedral two-component vesicles, we need to substitute the edges and vertices of the underlying polyhedral shape by structures representing the finite area fraction of soft material around them. This is done by replacing each edge by a piece of a cylinder mantle (with an angle matching the dihedral angle between the adjacent faces) and replacing each vertex by a piece of a sphere with a solid angle matching the vertex (angular) defect; see Fig. 2c for an example. Note that the the hard-material faces could be assembled to form a polyhedron in the conventional sense, while the soft material is filling the gaps between these faces.

2.4.1 Platonic Solids

The geometry of the five Platonic solids (the only perfectly regular, convex polyhedra) is known analytically²⁴. It is advantageous to express their properties in terms of the number of faces n and the coordination number c of the vertices: $c = 3$ for $n = 4, 6, 12$, while $c = 4$ for $n = 8$ and $c = 5$ for $n = 20$. The number of vertices per face is then

$$\eta = \frac{2c}{c-2} \left(1 - \frac{2}{n}\right). \quad (6)$$

The regular η -gons have an edge length, l , and c facets meet at one vertex with equal planar angle, $\alpha = \pi(1 - \frac{2}{\eta})$. The total number of edges and vertices are $E = \frac{n\eta}{2}$ and $V = \frac{n\eta}{c}$. The area of

an individual η -gon, a , can be calculated in terms of η , l , and α ,

$$a = \frac{\eta}{4} l^2 \tan\left(\frac{\alpha}{2}\right) \quad (7)$$

The dihedral angle θ between two facets is obtained by considering normal vectors of adjacent facets,

$$\theta = \cos^{-1}\left(\frac{1}{2}\left(-1 - 2\cos\left(\frac{2\pi}{c}\right) + \cos\alpha\right)\sec^2\left(\frac{\alpha}{2}\right)\right). \quad (8)$$

The radius r of the cylindrical and spherical parts of the soft-material phase is taken to be the same, in order to avoid a curvature discontinuity in the soft material region. As a result, A_s and $A_h = A_0 - A_s$ can be expressed in terms of l and r :

$$A_s = A_{s,cylinder} + A_{s,sphere} = E(\pi - \theta)rl + 4\pi r^2, \quad (9)$$

$$A_h = na = \frac{n\eta}{4} l^2 \tan\left(\frac{\alpha}{2}\right) \quad (10)$$

By definition, all sphere parts sum up to one complete sphere. The turning angle of each cylinder part is $\pi - \theta$ to satisfy the smoothness of the surface at the boundary between hard material and soft material. Expressions for $\bar{l} = l/\sqrt{A_0}$ and $\bar{r} = r/\sqrt{A_0}$ can be obtained by rearranging the above equations to yield

$$\bar{l} = \sqrt{\frac{4}{n\eta}(1-f)\cot\left(\frac{\alpha}{2}\right)}, \quad (11)$$

$$\bar{r} = \sqrt{\frac{E^2(\pi - \theta)^2 \bar{l}^2}{64\pi^2} + \frac{f}{4\pi} - \frac{E(\pi - \theta)\bar{l}}{8\pi}} \quad (12)$$

The total energy is now easily obtained taking into account that only the soft material contributes to the bending energy, and that the total boundary length between the phases is $n\eta l = 2El$. The dimensionless energy becomes

$$u_i = \bar{\kappa} \left[\frac{E(\pi - \theta)\bar{l}}{2\bar{r}} + 4\pi \right] + 2\bar{\Gamma}E\bar{l}, \quad (13)$$

where we use the subscript "i" to indicate the isotropy of the Platonic solids.

Figure 3 shows the resulting phase diagram in $\bar{\kappa} - \bar{\Gamma}$ space, at a fixed area fraction $f = 0.5$ (we shall investigate the dependence on f below). Indicated are the regions in which each of the shapes discussed (spherical – S, fragmented – F, polyhedral – indicated explicitly) is energetically the lowest; note that both axes are logarithmic. Unsurprisingly, fragmentation is favorable for large enough $\bar{\Gamma}$, while for $\bar{\kappa} \rightarrow 1$, the spherical solution is recovered for small enough $\bar{\Gamma}$ (this is the single-phase limit). The region of polyhedral shapes takes up the lower left of the diagram, where $\bar{\kappa}$ is small enough so that faceting of the hard material gives a large energetic benefit, while $\bar{\Gamma}$ is small enough so that the formation of the polyhedral soft phase (with its long inter-phase boundary) does not override this faceting benefit. We will show below that this general appearance of the phase diagram is very robust against changes in modeling.

Within the polyhedral region of the diagram, it is remarkable that octahedral and icosahedral solids are never energetically optimal – the entire region is taken up by tetrahedra, cubes, and

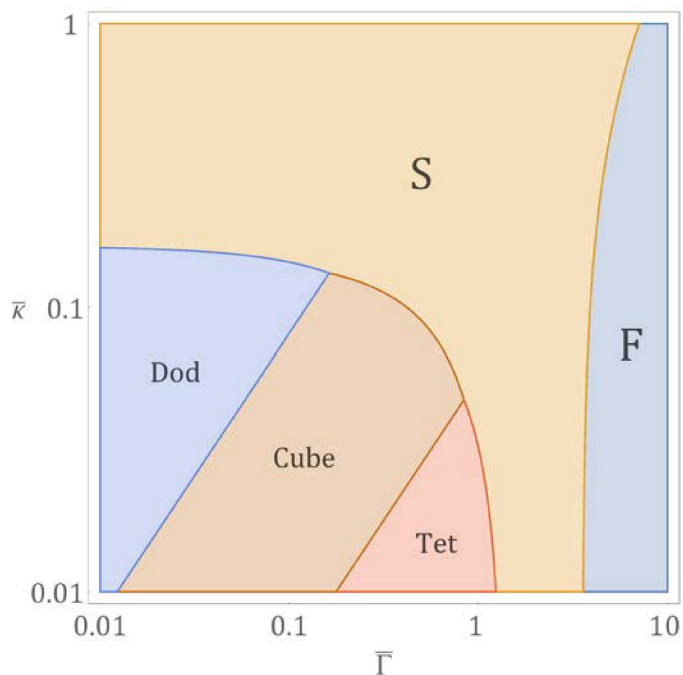


Fig. 3 Phase diagram indicating energetically lowest shapes, comparing Platonic solids with spherical shapes (S) and fragmented shapes (F) for $f = 0.5$. Only Platonic solids with $c = 3$ appear in the phase diagram: tetrahedra ($n = 4$), cubes ($n = 6$), and dodecahedra ($n = 12$).

dodecahedra, all with coordination number $c = 3$. We shall see below that this result is true for semiregular polyhedra as well: only $c = 3$ structures show up as lowest-energy states. This is intriguing because (i) icosahedra, the preferred shape of buckling induced by topological defects, are not only suppressed, but entirely absent; and (ii) the polyhedral ground states here are of a robust type – even in the low- f limit, a small perturbation to the structure will keep the coordination number at $c = 3$, while it will change for larger c . This indicates that polyhedral symmetries can be broken continuously.

This preference for $c = 3$ is straightforward to show analytically: the total energy of Platonic solids contains two linear terms, so it can be written as $u_i = C_\kappa(f, n, c)\bar{\kappa} + C_\Gamma(f, n, c)\bar{\Gamma}$. One finds that C_Γ and C_κ of the octahedron are larger than those of the cube for any f value, so that the cube is always energetically better than the octahedron. In the same way, the two coefficients of the icosahedron are always larger than those of the dodecahedron. Hence, it is sufficient to only consider Platonic solids with $c = 3$.

2.4.2 Isotropic Polyhedra and Area Fraction Dependence

One way of making analytical progress towards shapes of lesser symmetry is to compute averaged properties in the spirit of a mean-field model. While only the five Platonic solids exist, the formulas given above are well-defined as a function of n and c . The same conclusion as for Platonic solids holds for arbitrary n : the energies u_i for $c = 3$ are always lower than for higher coordination number. Thus, we analyze the model for arbitrary n at coordination number $c = 3$. This is inspired by work on polyhedral foam bubbles^{25,26}, for which it was shown that all geometrical

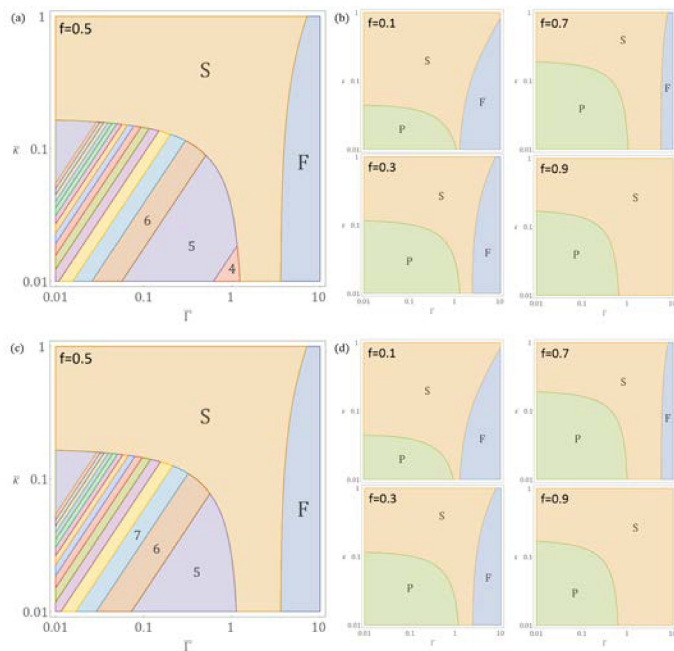


Fig. 4 (a) Phase diagram of isotropic polyhedra with constant area assumption and $f = 0.5$. The polyhedral region shows explicit results up to $n = 19$, with the optimal number of faces increasing as $\bar{\Gamma}$ increases and $\bar{\kappa}$ decreases. (b) Changes in the phase diagram of (a) with varying area fraction. All polyhedral shapes are indicated as region P. (c), (d) Phase diagrams of isotropic polyhedra with constant volume assumption. For all area fractions, the shape of the phase domains is not significantly different from the constant area model.

properties of typical polyhedra with n faces in a realistic setting are very closely matched by those obtained from the generalized- n formulas (foam bubbles always have $c = 3^{27}$). Figure 4a shows that there is indeed a continuous progression of the "optimal" face number, while the overall shape of the P region in the phase diagram is hardly changed over Fig. 3.

In Fig. 4b, we also see how the phase regions depend on the area fraction: For smaller f , fragmentation occurs at lower $\bar{\Gamma}$, as the bending energy penalty for fragmentation is less. The P region is only slightly affected by changes in f ; only for small f does it become significantly diminished at higher $\bar{\kappa}$: because of the strong curvature (small r) entailed by small f , a smaller $\bar{\kappa}$ is necessary to make faceting energetically favorable.

A very general feature observed in the polyhedral region of the phase diagram is the increasing number of facets n in the optimal polyhedron for lower $\bar{\Gamma}$ and higher $\bar{\kappa}$. As the total length of polyhedral edges grows as $n^{1/2}$, smaller $\bar{\Gamma}$ is necessary to stabilize larger n , while the higher n in turn leads to larger dihedral angles and relatively smaller contributions of edges to curvature energy. Therefore, the region for which a given n is energetically optimal stretches to higher $\bar{\kappa}$ for higher n . It has to be stressed that these isotropic polyhedra are not constructible for $n \neq 4, 6, 12$ and must be interpreted as typical mean-field representatives of a given n .

The isotropic polyhedra described here represent significant, but shallow energy minima: Evaluating the energy of an isotropic polyhedron with $n + 1$ or $n - 1$ faces for a combination of $\bar{\Gamma}$ and $\bar{\kappa}$ at the center of the region where n is the optimum number,

one finds that the relative energy differences are always less than 4% for all f and n values considered. This is similar to the analogous foam bubbles, the isotropic Plateau polyhedra, although those show even smaller energy variations of less than 1%²⁶. As in foam bubbles, the energy difference between neighboring face numbers becomes smaller as n increases, and asymptotically the relative deviation scales as $[u_i(n+1) - u_i(n)]/u_i(n) \propto 1/n$. Hence, we would expect polyhedral shapes at small n to be less susceptible to shape changes or trapping in local minima due to fluctuations.

2.4.3 Alternative Models and Comparison with Simulations

Are the shapes of the regions in the analytical phase diagrams robust with respect to changes in the modeling assumptions? We tested this question by changing the constraints of the analytical model from imposing constant area to imposing constant volume V_0 and using $V_0^{1/3}$ as the normalizing length scale. While we do not give the explicit formulas here, the energy contributions are computed in a similarly straightforward way to Section 2.4.1. The resulting phase diagrams are only very subtly changed (Fig. 4c, d): all qualitative features are entirely preserved, and the quantitative change in the phase boundaries is small (the P region $\bar{\kappa}(\bar{\Gamma})$ boundary differs by $\approx 5\%$ for moderate f values and less than 12% even for extreme f .) Furthermore, all optimal polyhedra are still three-fold coordinated. This shows that the precise nature of the energy functional is not important for the overall appearance of the phase diagram. This robustness had indeed been argued in the simulation work of SVO, where both area and volume elasticity had been implemented, with the outcomes only weakly dependent on the choice of moduli.

A quick estimate also shows that the assumption of constant area is appropriate for thin-shelled vesicles: The stretching energy for small area change is

$$U_{stretch} = \frac{1}{2} K_A \int \left(\frac{\Delta A}{A} \right)^2 dA, \quad (14)$$

if $\Delta A/A$ is the local area strain. From the elasticity theory of a homogeneous thin layer, the relation between the bending modulus and the area stretch modulus is $K_A = \frac{12\kappa_b}{h^2}$, where h is the shell thickness. Assuming uniform stretch, the non-dimensional stretching energy of a hard-material sphere is

$$u_{stretch} = 24\pi \left(\frac{R}{h} \right)^2 \left(\frac{\Delta A}{A} \right)^2 \quad (15)$$

A truly thin shell in practical vesicle applications typically has $\frac{R}{h} \sim 10^2 - 10^3$. In order to balance or surpass the O(1) bending and line energies defined above, $\Delta A/A$ only needs to exceed $10^{-4} - 10^{-3}$. Hence, the constant area assumption is accurate; in the following, we continue to discuss the implications of the constant-area model and compare its predictions directly with those of SVO.

The simulations of SVO did not allow for fragmentation into more than one vesicle, so that there is no direct analogue of the "F" regions in our phase diagrams. The lack of fragmentation is related to the way line tension was implemented in the nu-

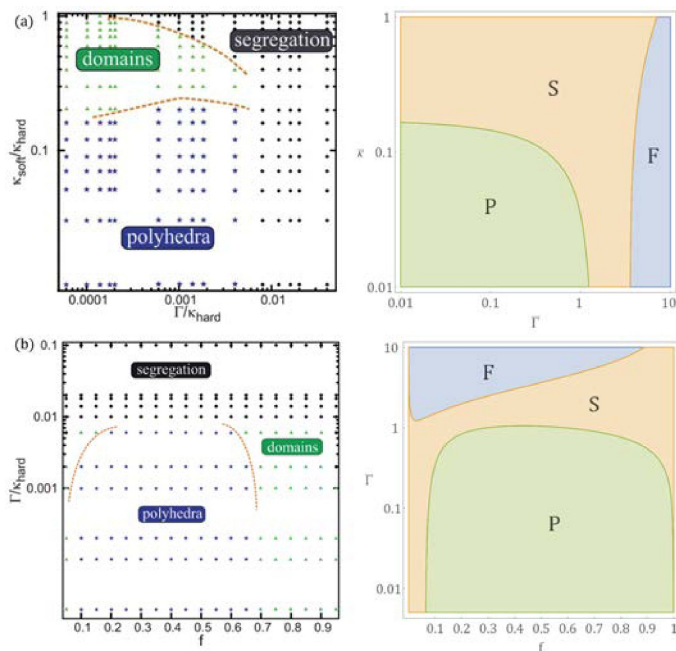


Fig. 5 Comparison between the numerical simulations of SVO (left) and the present theoretical model (right). The phase diagrams show (a) $\bar{\kappa}$ and $\bar{\Gamma}$ for $f = 0.5$; (b) $\bar{\Gamma}$ and f for $\bar{\kappa} = 0.03$.

merics, where the number of simulation contact sites between domains was penalized, but not physical length of the boundary. The numerical parameter in the phase diagrams of SVO is " Γ/κ_{hard} ", where Γ represents an energy, not a line tension. The values are based on a computational mesh (lattice) of unit distance, and a vesicle whose radius R is 11.5 times that distance²¹. Furthermore, κ_{hard} is a numerical bending modulus in a triangular grid, which is related to the continuum bending modulus κ_h by $\kappa_h/\kappa_{hard} = \sqrt{3}/2$ ²⁸. This demonstrates that, for comparison of " Γ/κ_{hard} " from SVO with our dimensionless line tension ($\bar{\Gamma} = \Gamma\sqrt{A_0}/\kappa_h$), the former needs to be multiplied by $k = 4m\sqrt{\pi/3} \times 11.5$, where m is the mean number of intersections of mesh edges across the boundary between the two phases, per mesh edge length. A straightforward calculation shows that for a regular triangular mesh (unit edge length), this number is

$$m = \frac{1}{\sqrt{3}\pi} \int_0^{2\pi} (|\sin\phi| + |\sin(\phi + \pi/3)| + |\sin(\phi - \pi/3)|) d\phi = 4\sqrt{3}/\pi \approx 2.205. \quad (16)$$

This means the multiplication factor between the numerical and analytical axes of line tension is $k \approx 103.8$. Figure 5 shows that, indeed, the axis values are about two orders of magnitude different. Consulting figure 5 of SVO affords a somewhat more quantitative estimate: for $f = 0.5$, fully segregated (spherical) shapes are obtained for $\Gamma/\kappa_{hard} \gtrsim 0.01$, where the phase boundary location is made explicit for a bending modulus ratio of $\bar{\kappa} = 0.03$. In our model this boundary value is $\bar{\Gamma} \approx 1.04$, in essentially exact agreement with the factor k above.

Not everywhere in the phase diagrams of SVO is the boundary between P and S regions as clear, however. The simulations designate another class of shapes as "domains", indicating cases

where the hard components form multiple domains (no complete segregation), but where the overall shape of the vesicle was not clearly polyhedral. There was no quantitative criterion employed to define the "domain" state, but it was assigned by visual inspection (R. Sknepnek, personal communication). In particular for larger f , the large surface area covered by soft, rounded structures means that all structures with a polyhedral pattern of hard-material patches were classified as "domains". Conversely, the limit of $\bar{\kappa} \rightarrow 1$ blurs the distinction between the materials and provides a very low energy threshold between full segregation and smaller domains – in these cases, the true lowest-energy state may be that of segregation, but it may not be reached within accessible computational times.

The latter distinction is on display in the comparison of Fig. 5a for a fixed $f = 0.5$. There is very good agreement concerning the vertical boundary between P and S regions of the $\bar{\kappa} - \bar{\Gamma}$ phase diagram (at $\bar{\Gamma} \approx 1$), and the horizontal boundary becomes equally well described when the domain regions are interpreted as belonging to S. Conversely, in the $\bar{\Gamma} - f$ diagram of Fig. 5b, it is the horizontal and left-hand vertical boundaries that are well-represented, while the large- f structures classified as "domains" in the simulation should be interpreted as polyhedral (with a very wide soft-phase area around each edge). The overall appearance of the phase diagram is qualitatively and semi-quantitatively reproduced by the theory, and the quantitative agreement along the unambiguous P-S boundary encourages further exploration of the theory's predictions for polyhedral shapes.

Yet another approach investigated in a paper precedent to SVO²⁰ shows qualitatively similar equilibrium shapes as well. In that work, two-component vesicles with different stretch and bending moduli in the two phases are simulated, but without line tension. Consequently, the soft lattice elements tend to form single-width edges to reduce the high bending energy of the hard material for small f , so that polyhedral structures are formed. These are reported to often lack maximum symmetry²⁰ and to prefer three-fold edge coordination, again in agreement with the present work. By contrast, at moderate to large f , isolated soft-lattice sites are located randomly on the flat facet regions in²⁰ and a continuous soft phase fails to form, as line tension does not promote cohesive separate domains. Nevertheless, this work is another indication that non-icosahedral polyhedra of reduced symmetry are a common feature of two-component systems regardless of the details of the energy functional.

3 Breaking Polyhedral Symmetries

In deriving the formulas for isotropic polyhedra of arbitrary face number n above, we were inspired by work in foams²⁶, where an analogous method showed very good agreement with real (actually constructible) polyhedra of the same n . However, it is also known that there are greater differences in geometry (and overall energy) between isotropic and real foam polyhedra for small n , where the detailed arrangement of facets has a larger effect on overall energy. In particular, it was found that some polyhedra with small face number can reach energetically lower states than their isotropic analogs, whether constructible or not (Andrew M. Kraynik, personal communication). To probe whether irregular

polyhedra can be energetically favorable over isotropic polyhedra for two-component vesicles, we now turn to other classes of polyhedral shapes.

3.1 Semiregular Polyhedra

The semiregular polyhedra comprise, apart from the Platonic solids, all 13 Archimedean solids and semiregular upright prisms (those with equal edge lengths)²⁹. All of their geometries are known in closed form and result in formulas similar to those in Section 2.4.1; explicitly, we obtain the total energy as

$$u_a = \bar{\kappa} \left[\sum_j \frac{E_{a,j}(\pi - \theta_{a,j})\bar{l}_a}{2\bar{r}_a} + 4\pi \right] + 2\bar{\Gamma} \sum_j E_{a,j}\bar{l}_a, \quad (17)$$

where the index j counts the different types of adjacent-face occurrences. The dimensionless edge length (universal for each Archimedean solid) is

$$\bar{l}_a = \sqrt{\frac{(1-f)}{m_a}} \quad (18)$$

with m_a satisfying the relation $A_h/A_0 = m_a\bar{l}_a^2$. The soft-phase radius is given by

$$\bar{r}_a = \sqrt{\frac{\sum_j E_{a,j}^2 (\pi - \theta_{a,j})^2 \bar{l}_a^2}{64\pi^2} + \frac{f}{4\pi}} - \frac{\sum_j E_{a,j} (\pi - \theta_{a,j}) \bar{l}_a}{8\pi}. \quad (19)$$

For instance, the truncated tetrahedron has 8 facets (4 equilateral triangles and 4 regular hexagons), as shown in Fig. 1c. The dihedral angle at the edge between a triangle and a hexagon is $\theta_{a,1} = \cos^{-1}(-\frac{1}{3})$ and that between two hexagons is $\theta_{a,2} = \cos^{-1}(\frac{1}{3})$. There are $E_{a,1} = 12$ and $E_{a,2} = 6$ edges of these types, respectively, and $m_A = 7\sqrt{3}$. The total energy follows from the above equation as

$$u_{a,t} = \bar{\kappa} \left[4\pi + \frac{(9\pi - 6\theta_{t,1} - 3\theta_{t,2})\bar{l}_t}{\bar{r}_t} \right] + \bar{\Gamma} \left[36\sqrt{\frac{1-f}{7\sqrt{3}}} \right], \quad (20)$$

with

$$\bar{l}_t = \sqrt{\frac{1-f}{7\sqrt{3}}} \quad (21)$$

and

$$\bar{r}_t = \frac{1}{2} \left[\sqrt{\left(\frac{9}{2} - \frac{3\theta_{t,1}}{\pi} - \frac{3\theta_{t,2}}{2\pi} \right)^2 \bar{l}_t^2 + \frac{f}{\pi}} - \left(\frac{9}{2} - \frac{3\theta_{t,1}}{\pi} - \frac{3\theta_{t,2}}{2\pi} \right) \bar{l}_t \right]. \quad (22)$$

Comparing the u_a values with the u_i above, the phase diagrams are altered wherever one of the non-Platonic shapes has a lower energy. Again, we find that only structures with $c = 3$ ever show up as energetically optimal, for similar reasons as before. This leaves seven Archimedean solids with $c = 3$ and the semiregular upright prisms with regular polygons of $\eta_{pr} = 3, 5, 6, \dots$ ($\eta_{pr} = 4$ is the cube). But intriguingly, of these semiregular polyhedra, only two generate a lower-energy state than the regular polyhedra considered before: the two structures with the lowest n in their subclass, the triangular prism ($n = 5$) and the truncated tetrahedron ($n = 8$). As shown in Fig. 6a for $f = 0.5$, these poly-

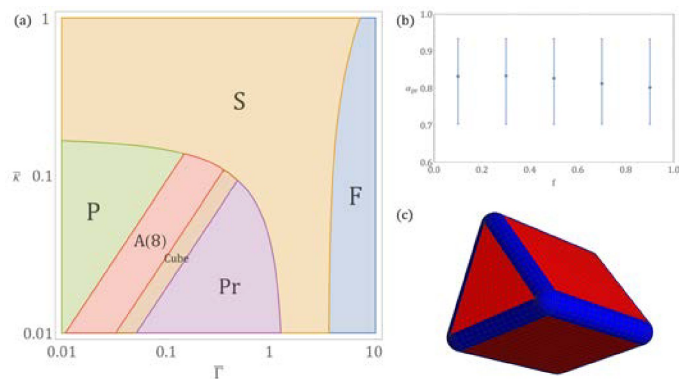


Fig. 6 (a) Phase diagram containing isotropic polyhedra and semiregular polyhedra. Only two semiregular polyhedra appear on the phase diagram: the triangular prism (Pr) and the truncated tetrahedron A(8). The Pr region is not visibly changed when irregular prisms of arbitrary aspect ratio α_{pr} are included. (b) The range of optimal α_{pr} for irregular prisms is almost independent of f . (c) Representative example of a general prism with $\alpha_{pr} = 0.8$.

hedra actually exclude the (regular) tetrahedron from the phase diagram. A small stripe between their domains indicates combinations of $(\bar{\Gamma}, \bar{\kappa})$ for which the cube is still optimal. At larger n , however, isotropic polyhedra (whether real Platonic solids or mean-field constructs) remain energetically favorable. Nevertheless, in a significant part of the polyhedral phase diagram is the most symmetric structure not the energetically lowest, confirming our hypothesis that irregularity becomes more important (for low-energy polyhedra) at small face number.

3.2 General Prisms

We explore the above-mentioned hypothesis further, asking whether additional symmetry breaking will result in polyhedra of even lower energy. This is relatively easy to execute for prismatic shapes: while the semiregular prisms above are characterized by equal edge lengths (the edge lengths l_{pr} on the polygonal end faces are equal to the height h_{pr} of the prism), all formulas can be evaluated for arbitrary aspect ratios $\alpha_{pr} = l_{pr}/h_{pr}$. The additional optimization parameter α_{pr} potentially allows the energy to be lowered. We focus on the triangular prism here (the only one that proved optimal in the phase diagram above); the corresponding areas of hard material and soft material can be written in terms of h_{pr} , l_{pr} , and r_{pr} ,

$$A_h = \frac{\sqrt{3}}{2} l_{pr}^2 + 3h_{pr}l_{pr}, \quad (23)$$

$$A_s = 2\pi r_{pr}h_{pr} + 3\pi r_{pr}l_{pr} + 4\pi r_{pr}^2. \quad (24)$$

As the dihedral angle between a triangle and a rectangle is $\frac{\pi}{2}$ and that between two rectangles is $\frac{\pi}{3}$, the total energy follows as

$$u_{pr} = \bar{\kappa} \left[4\pi + \frac{3\pi\bar{l}_{pr}}{2\bar{r}_{pr}} + \frac{\pi\bar{h}_{pr}}{\bar{r}_{pr}} \right] + \bar{\Gamma} [12\bar{l}_{pr} + 6\bar{h}_{pr}], \quad (25)$$

where

$$\bar{l}_{pr} = \sqrt{3\bar{h}_{pr}^2 + \frac{2}{\sqrt{3}}(1-f)} - \sqrt{3}\bar{h}_{pr} \quad (26)$$

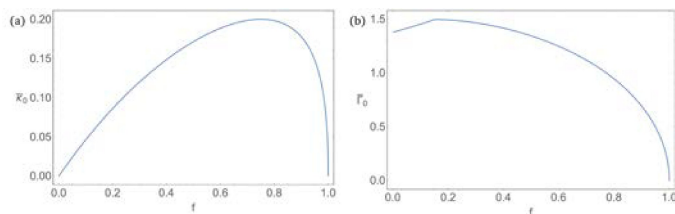


Fig. 7 (a) Asymptotic values $\bar{\kappa}_0$ of $\bar{\kappa}$ at vanishing $\bar{\Gamma}$. (b) Asymptotic values $\bar{\Gamma}_0$ of $\bar{\Gamma}$ at vanishing $\bar{\kappa}$.

and

$$\bar{r}_{pr} = \frac{1}{2} \left[\sqrt{\left(\frac{\bar{h}_{pr}}{2} + \frac{3\bar{l}_{pr}}{4}\right)^2 + \frac{f}{\pi}} - \left(\frac{\bar{h}_{pr}}{2} + \frac{3\bar{l}_{pr}}{4}\right) \right] \quad (27)$$

For a given $\bar{\kappa}$ and $\bar{\Gamma}$, a unique α_{pr} value can be determined to minimize the total energy. One finds that, indeed, a prism with $\alpha \neq 1$ is the energetically lowest for all $(\bar{\kappa}, \bar{\Gamma})$, although the values only vary between 0.7 and 0.94, with a mean of about $\alpha \approx 0.8$ (Fig. 6b,c). These irregular triangular prisms beat the energy of semiregular prisms; in a very small parameter, they are also energetically lower than the cube, but the resulting extension of the Pr region in Fig. 6 is so slight as to be invisible if plotted. Overall, these irregular prismatic shapes are energetically lower than any more regular polyhedral shape in a rather broad range of parameters, for moderate $\bar{\Gamma}$ and small enough $\bar{\kappa}$. It is also noteworthy that any shape transition between spherical and polyhedral shapes will be the most abrupt (involve the largest change in configuration) at this boundary where $n = 5$ triangular prisms are the preferred polyhedral shape. This may compromise the accessibility of this particular ground state in a dynamical situation.

4 Phase Boundaries

Given the relative simplicity and explicit nature of the energy formulas, further insight into the location of the boundaries between the S, F, and P regions can be obtained. Except for small f , the fragmentation region F only bounds the spherical region S, and the boundary can be written analytically by equating the total energy values, $u_{sph} = u_{frag}$. The result is a linear relation between $\bar{\kappa}$ and $\bar{\Gamma}$ at the boundary,

$$4\pi(1-f)\bar{\kappa} + 4\pi f - \bar{\Gamma}\sqrt{4\pi f(1-f)} = 0. \quad (28)$$

In the physical system, the vesicle undergoes budding in order to achieve complete fragmentation. Although the current analysis does not provide a prediction of an intermediate budding shape, it qualitatively shows that the budding and the fragmentation of heterogeneous vesicle is encouraged by strong line tension. In the limit of $\bar{\kappa} \rightarrow 1$ (single-component vesicle), the critical $\bar{\Gamma}$ for fragmentation is equal to $\sqrt{4\pi}/\sqrt{f(1-f)}$.

At the phase boundary between the polyhedra mode and the sphere region, total energy values for these two modes are likewise equal. While the exact shape of the boundary depends on the kind of polyhedron considered, the differences are very slight. We will therefore use the isotropic-polyhedra formulas (6) – (13) for evaluation. Specifically, the phase boundary is the envelope of

the family of curves $u_{sph}(\bar{\Gamma}, \bar{\kappa}) = u_i(\bar{\Gamma}, \bar{\kappa}, n)$, i.e., it is given by the system of equations

$$u_{sph}(\bar{\Gamma}, \bar{\kappa}) - u_i(\bar{\Gamma}, \bar{\kappa}, n) = 0, \quad \partial u_i(\bar{\Gamma}, \bar{\kappa}, n)/\partial n = 0. \quad (29)$$

The resulting expressions (involved, but analytically known) give a parametric representation of the phase boundary $(\bar{\Gamma}(n), \bar{\kappa}(n))$.

It is also instructive to compute the asymptotes of the polyhedral region in the limits of $\bar{\kappa} \rightarrow 0$ and $\bar{\Gamma} \rightarrow 0$. These prescribe the extent of the P region, which (as shown above) is robust against changes in modeling assumptions. As $\bar{\Gamma}$ approaches zero, the corresponding face number n goes to infinity and the asymptotic value of $\bar{\kappa}$ follows as (Fig. 7a)

$$\bar{\kappa}_0 = \frac{(f-1)(1-\sqrt{1-f})}{f-1-f\sqrt{1-f}} \quad (30)$$

$\bar{\kappa}_0$ vanishes at both $f = 0$ and $f = 1$. The bending energy of the polyhedra mode diverges as $f \rightarrow 0$, so the sphere mode is energetically better no matter what the value of $\bar{\kappa}$ is. Conversely, any concentration of bending energy is energetically costly when $f \rightarrow 1$. $\bar{\kappa}_0$ has a maximum value at $f_0 = 3/4$. At f_0 , the polyhedral shape range along the $\bar{\kappa}$ axis is greatest, and we predict that this area fraction should be the most advantageous for the generation of polyhedral vesicles at small line tension.

The other asymptote is given by $\bar{\kappa} = 0$. Formally, this happens when $n = 3$, but there is no constructible 3-faced isotropic shape; therefore, $n = 4$ is the smallest realistic value. For small enough f , the shape transition occurs between the P and F regions instead of between the P and S regions (cf. the $f = 0.1$ phase diagram in Fig 4b). The critical area fraction f_i can be calculated by comparing total energies and it is found that $f_i \approx 0.15115$. In summary, we have

$$\bar{\Gamma}_0 = \begin{cases} \frac{2\pi(f-1)}{\sqrt{\pi f(1-f)} - 2 \times 3^{3/4} \sqrt{1-f}} & f > f_i \\ \frac{\pi}{3^{3/4} \sqrt{1-f}} & 0 < f \leq f_i, \end{cases} \quad (31)$$

and $\bar{\Gamma}_0$ is maximal for $f = f_i$ (see Fig. 7b). $\bar{\Gamma}_0$ does not approach to 0 even when $f \rightarrow 0$. No matter how small f is, there always exists a boundary between soft material and hard material in the P regime while the total energy of the fragmentation shape is constant if $\bar{\kappa} = 0$. Setting $f = 0$ in (31), we obtain $\bar{\Gamma}_0(f = 0) = \frac{\pi}{3^{3/4}}$.

5 Conclusions

An evaluation of a common free energy functional for two-component vesicles for various analytically known shapes has yielded robust predictions for the occurrence of polyhedral shapes in the parameter space of line tension, bending modulus ratio, and area fraction. The two distinct materials separate completely when the line tension is sufficiently dominant. For intermediate values of the line tension, the vesicle maintains a spherical shape but the domains of the soft and hard materials segregate completely. For small enough line tension and large enough bending modulus ratio this spherical solution is not optimal and gives way to polyhedral solutions. In contrast to buckling by geometrical frustration, icosahedral shapes are never the shapes of lowest energy, and in fact only polyhedra with coordination number three

are found to be equilibrium shapes.

Isotropic polyhedra, while of maximum symmetry, are energetically preferable only in a relatively small region of parameter space, requiring small line tension and a bending modulus ratio close to the one inducing segregation of the phases. Instead, we find that breaking symmetries (making the polyhedra more irregular) actually results in shapes of lower total energy at low face number. This is true for the truncated tetrahedron (an Archimedean solid), reminiscent of shapes observed in carboxysomes¹⁵, and also for prismatic shapes, with we predict to be prevalent at larger line tensions. Regular tetrahedral isotropic shapes are not optimal within this model, although different types of interaction between constituents (e.g nematic states³) can stabilize such polyhedra. The successive improvement of energy upon breaking of symmetries suggests that some of the experimentally observed irregular shapes may be the result not of statistical variation, but of deterministic energy minimization.

The theoretical model can be potentially applied to other vesicular structures like a thin elastic shell or virus capsid. It is not confined to lipid bilayer membranes and we have shown that significant changes in the modeling assumptions have very little effect on the overall appearance of parameter space regions, as long as the main energy balance between bending and line tension is maintained. An analogous study is easy to do for a modified energy functional with other dominant energy contributions as well. Our results indicate general correlations between the shape of a vesicle and its mechanical properties; thus, certain shapes can be deliberately generated by carefully tuning the physical properties and the relative composition of the materials. Conversely, a range of material properties can be predicted from the vesicle shape observed in experiment.

Although the present analysis explains the vesicle shape transition semi-quantitatively, it has several limitations. For a given combination of parameters, our results show the ground state shape only; in practice, the vesicle does not always succeed in annealing to the ground state. A large variety of vesicle shapes shown in both experiments and numerical simulations may be the result of local energy minima. Furthermore, other shape modes that we did not quantify here may lead to lower energy – having shown that breaking symmetries can lead to improved energy, it is natural to wonder whether entirely irregular structures might succeed in lowering the energy further. Experimental results seem to generally show polyhedra of a certain regularity, however. We also remark that the simplified geometry of flat faces, cylindrical edge structures, and spherical vertex regions is likely to lead to systematic errors with respect to realistic vesicles shapes that might be a concern at large fractions of the soft phase. Finally, thermal effects are not taken into account here but can be significant on the vesicle scale, which is often in the micron and sub-micron range. Thermal fluctuations may blur the phase boundaries in certain cases if the differences in energy between structures are smaller than typical thermal energies. All of these caveats can and should be addressed in future work, as they are relatively straightforward to implement into the formalism presented here. The observation of polyhedral vesicle shapes, and in particular the occurrence of less regular polyhedra, has been a

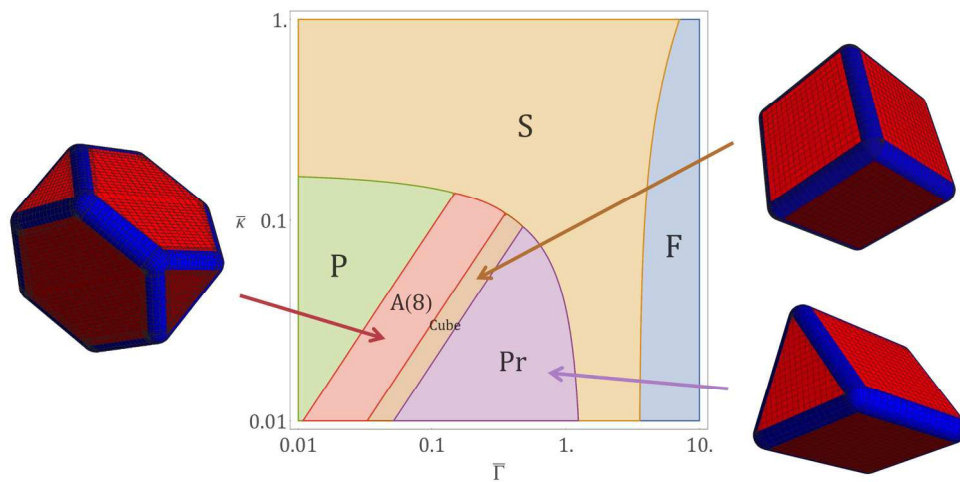
source of initial puzzlement, but modeling like the present theory contributes to improving our ability to predict and interpret such shapes, and eventually put them to use in applications.

Acknowledgments: The authors thank Monica Olvera de la Cruz and Zhenwei Yao for constructive discussions, and Rastko Sknepnek and Andrew Kraynik for providing helpful information through personal communication. We gratefully acknowledge support from the NIH grant R01 GM098077 "Tissue Morphogenesis: A study of Molecular Machines and Cell Mechanics".

References

- 1 W. Helfrich, *Zeitschrift für Naturforschung. Teil C: Biochemie, Biophysik, Biologie, Virologie*, 1973, **28**, 693–703.
- 2 B. L. Scola, S. Audic, C. Robert, L. Jungang, X. de Lamballerie, M. Drancourt, R. Birtles, J.-M. Claverie and D. Raoult, *Science*, 2003, **299**, 2033.
- 3 X. Xing, H. Shin, M. J. Bowick, Z. Yao, L. Jia and M.-H. Li, *Proceedings of the National Academy of Sciences*, 2012, **109**, 5202–5206.
- 4 â. Filipe E. Antunes, â. Rodrigo O. Brito, â. Eduardo F. Marques, *, Â. BjÄrn Lindman, âÄ, and M. MiguelâÄ, *The Journal of Physical Chemistry B*, 2007, **111**, 116–123.
- 5 J. Lidmar, L. Mirny and D. Nelson, *Phys. Rev. E*, 2003, **68**, 051910.
- 6 K. Zahn and G. Maret, *Physical review letters*, 2000, **85**, 3656.
- 7 A. Mughal and M. Moore, *Physical Review E*, 2007, **76**, 011606.
- 8 Z. Yao and M. O. de la Cruz, *Physical review letters*, 2013, **111**, 115503.
- 9 Z. Yao and M. O. de la Cruz, *Proceedings of the National Academy of Sciences*, 2014, **111**, 5094–5099.
- 10 M. J. Bowick and L. Giomi, *Advances in Physics*, 2009, **58**, 449–563.
- 11 U. Seifert and R. Lipowsky, *Structure and Dynamics of Membranes From Cells to Vesicles*, North-Holland, 1995, vol. 1, pp. 403 – 463.
- 12 M. A. Greenfield, L. C. Palmer, G. Vernizzi, M. O. d. l. Cruz and S. I. Stupp, *Journal of the American Chemical Society*, 2009, **131**, 12030–12031.
- 13 C.-Y. Leung, L. C. Palmer, B. F. Qiao, S. Kewalramani, R. Sknepnek, C. J. Newcomb, M. A. Greenfield, G. Vernizzi, S. I. Stupp, M. J. Bedzyk and M. Olvera de la Cruz, *ACS Nano*, 2012, **6**, 10901–10909.
- 14 A. K.-C. So, G. S. Espie, E. B. Williams, J. M. Shively, S. Heinrich and G. C. Cannon, *Journal of Bacteriology*, 2004, **186**, 623–630.
- 15 C. Fan, S. Cheng, Y. Liu, C. M. Escobar, C. S. Crowley, R. E. Jefferson, T. O. Yeates and T. A. Bobik, *Proceedings of the National Academy of Sciences*, 2010, **107**, 7509–7514.
- 16 Reinhard Lipowsky, *J. Phys. II France*, 1992, **2**, 1825–1840.
- 17 F. Jülicher and R. Lipowsky, *Phys. Rev. E*, 1996, **53**, 2670–2683.
- 18 P. B. Sunil Kumar, G. Gompper and R. Lipowsky, *Phys. Rev. Lett.*, 2001, **86**, 3911–3914.

- 19 J. Hu, T. Weigl and R. Lipowsky, *Soft Matter*, 2011, **7**, 6092–6102.
- 20 G. Vernizzi, R. Sknepnek and M. Olvera de la Cruz, *Proceedings of the National Academy of Sciences*, 2011, **108**, 4292–4296.
- 21 R. Sknepnek, G. Vernizzi and M. Olvera de la Cruz, *Soft Matter*, 2012, **8**, 636–644.
- 22 U. Seifert, K. Berndl and R. Lipowsky, *Phys. Rev. A*, 1991, **44**, 1182–1202.
- 23 D. H. Boal, *Mechanics of the Cell*, Cambridge University Press, 2012.
- 24 H. Steinhaus, *Platonic Solids, Crystals, Bees' Heads, and Soap. Ch 8 in Mathematical snapshots 3rd Ed.*, New York:Dover, 1999, pp. 191 – 201.
- 25 S. Hilgenfeldt, A. M. Kraynik, S. A. Koehler and H. A. Stone, *Phys. Rev. Lett.*, 2001, **86**, 2685–2688.
- 26 S. Hilgenfeldt, A. M. Kraynik, D. A. Reinelt and J. M. Sullivan, *EPL (Europhysics Letters)*, 2004, **67**, 484.
- 27 D. L. Weaire and S. Hutzler, *The physics of foams*, Oxford University Press, 2001.
- 28 H. S. Seung and D. R. Nelson, *Phys. Rev. A*, 1988, **38**, 1005–1018.
- 29 H. Coxeter, *Mathematische Zeitschrift*, 1940, **46**, 380–407.



The equilibrium shapes of vesicles made from hard (red) and soft (blue) components are found to prefer lesser symmetry (e.g. prisms rather than cubes) over a wide range of parameters.
 312x148mm (192 x 192 DPI)